SUPRAMOLECULAR CHEMISTRY

10.1126/sciadv.1500827

Spontaneous structural transition and crystal formation in minimal supramolecular polymer model

Galit Fichman,[1]* Tom Guterman,[1] Joshua Damron,[2] Lihi Adler-Abramovich,[1,3] Judith Schmidt,[4] Ellina Kesselman,[4] Linda J. W. Shimon,[5] Ayyalusamy Ramamoorthy,[2] Yeshayahu Talmon,[4] Ehud Gazit[1,6†]

The association of building blocks into supramolecular polymers allows the fabrication of diverse functional architectures at the nanoscale. The use of minimal assembly units to explore polymer dynamics and phase transitions significantly contributes to the application of polymer physicochemical paradigms in the field of supramolecular polymers. We present a minimal model that displays spontaneous coordinated structural transitions between micro- and nanostructures, hydrogels with nanoscale order, and single crystals. The simple amphiphilic 9-fluorenylmethoxycarbonyl-3,4-dihydroxyphenylalanine (Fmoc-DOPA) modified amino acid undergoes a noninduced transition from spherical assemblies into nanofibrils followed by sol-gel transition, nanotube formation via intermediate assembly, and crystallization within the gel. Notably, the transition kinetics is slow enough to allow both multistage and multiscale characterization of the supramolecular arrangement using electron microscopy, vibrational and circular dichroism spectroscopies, nuclear magnetic resonance, and x-ray crystallography. This minimalistic system is the first comprehensive model for a complete spontaneous structural transition between diverse states governed by distinct molecular interactions.

INTRODUCTION

Supramolecular polymers are organized arrays of monomeric units associated by highly directional noncovalent interactions (*1*–*3*). In the last decade, these assemblies have attracted considerable attention due to their valuable functionality. Owing to the dynamic and reversible nature of supramolecular systems, these polymers display unique properties, including responsiveness to stimuli, environmental adaptation, tunable degradability, and self-healing, making them excellent candidates to act as "smart materials" for various applications (*4*–*11*). Much effort has been made to investigate the elusive aspects of supramolecular systems (*5*, *12*), with emphasis on the mechanisms underlying noncovalent associations in living systems, far from thermodynamic equilibrium (*13*–*17*), as well as on the elucidation of the dynamic nature of assembly processes and their relation to polymer functionality (*18*). Specifically, events of extended time scale that involve internal reorganization are of immense interest (*19*–*21*).

To explore the physicochemical and structural dynamics of supramolecular assemblies, simple model systems should be established. Various building blocks, most notably amphiphilic molecules, were reported to form such assemblies (*19*, *20*, *22*, *23*). Aromatic peptide and amino acid amphiphiles are especially interesting simple building blocks that self-assemble into a variety of functional assemblies (*24*–*26*). In such systems, hydrophobic interactions, and especially interactions between planar and rigid aromatic moieties enable the formation of highly ordered assemblies from remarkably small building blocks (*27*–*31*). One such building block, the 9-fluorenylmethoxycarbonyl-3,4-dihydroxyphenylalanine (Fmoc-DOPA; Fig. 1A), a modified aromatic amino acid amphiphile, was recently reported to form ordered nanofibrillar structures (*32*).

Fmoc-DOPA molecules have the ability to form various intermolecular directional interactions, including hydrophobic interactions, hydrogen bonding, and π-π stacking, which allow the formation of diverse classes of supramolecular assemblies. Furthermore, this building block has the potential to form hydrogels, similarly to other Fmoc-modified aromatic amino acids, including Fmoc-tyrosine (*33*, *34*), Fmoc-phenylalanine (*34*, *35*), and Fmoc-pentafluorophenylalanine (*36*), which were proven to be efficient low–molecular weight (LMW) hydrogelators (*37*). The sol-gel transition, where monomeric soluble units transform into ordered arrays of fibrillar nanostructures as part of the gel matrix, can further assist in monitoring the supramolecular polymerization. The ability of Fmoc-DOPA to act as a hydrogelator was recently reported by Mezzenga and co-workers (*32*), who described the assembly of Fmoc-DOPA building blocks in water at low pH into fibrillar assemblies that led to the formation of a hydrogel with low mechanical rigidity.

Here, Fmoc-DOPA represents an exceptionally minimal model for supramolecular polymers that undergo noninduced transitions between alternative morphologies that are governed by distinct molecular forces at the different stages. We examined the assembly of Fmoc-DOPA using light and electron microscopy, spectroscopy, solution and solid-state nuclear magnetic resonance (ssNMR), and x-ray crystallography. We report that Fmoc-DOPA undergoes a multistage structural transition from spheres to ribbons, fibers, helices, and nanotubes. Moreover, the assembly process involves phase transition at the macroscopic level with a sol-gel alteration that culminates in the formation of crystals. Despite its apparent simplicity, Fmoc-DOPA participates in complex, spontaneous structural transitions with intermediate metastable assemblies. The remarkably small size of this building block, together with

[1]Department of Molecular Microbiology and Biotechnology, George S. Wise Faculty of Life Sciences, Tel Aviv University, Tel Aviv 6997801, Israel. [2]Biophysics and Department of Chemistry, University of Michigan, Ann Arbor, MI 48109–1055, USA. [3]Department of Oral Biology, The Goldschleger School of Dental Medicine, Tel Aviv University, Tel Aviv 6997801, Israel. [4]Department of Chemical Engineering, Technion—Israel Institute of Technology, Haifa 32000, Israel. [5]Department of Chemical Research Support, Weizmann Institute of Science, Rehovot 76100, Israel. [6]Department of Materials Science and Engineering, Iby and Aladar Fleischman Faculty of Engineering, Tel Aviv University, Tel Aviv 6997801, Israel.
*Present address: Chemical Biology Laboratory, National Cancer Institute, National Institutes of Health, Frederick, MD 21702, USA.
†Corresponding author. E-mail: ehudg@post.tau.ac.il

the dynamic nature of its assembly process, makes this system a minimalistic yet comprehensive model for supramolecular polymerization.

RESULTS AND DISCUSSION

Macroscopic view and imaging of Fmoc-DOPA assembly

The self-assembly of Fmoc-DOPA was triggered by the solvent switch of Fmoc-DOPA ethanol stock solution (100 mg/ml) into water. This was accompanied by three observable macroscopic changes. First, the dilution of the stock solution into water was associated with a turbidity change, that is, the solution instantly became opaque and then gradually became clearer (fig. S1). The second change concerns the viscoelastic properties of the preparation, where gel-like characteristics, as indicated by a simple qualitative vial inversion assay, appeared within hours (Fig. 1B). A later, third macroscopic change was the spontaneous appearance of crystals in the gel within weeks (Fig. 1B).

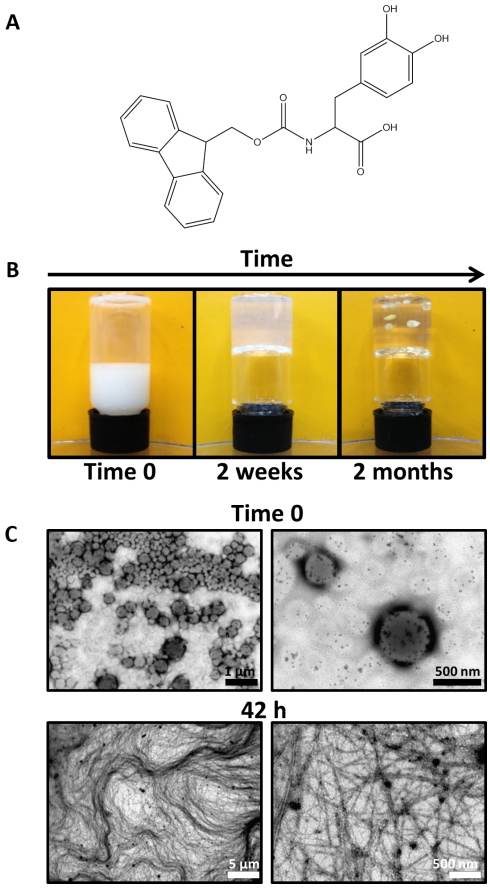

Fig. 1. Macroscopic view and imaging of Fmoc-DOPA assembly process. (**A**) Chemical structure of Fmoc-DOPA. (**B**) Three macroscopically observable changes of Fmoc-DOPA preparation over time: turbidity change, gaining gel-like viscoelastic characteristics as indicated by a simple qualitative vial inversion assay, and spontaneous formation of crystals in the gel (from left to right). (**C**) Transmission electron microscopy (TEM) micrographs of Fmoc-DOPA samples taken immediately upon the initiation of assembly (time 0) and 42 hours after the initiation of the assembly at the semitransparent gel-like state.

The assembly process was monitored at higher resolution by carrying out the assembly inside a sealed capillary while continuously imaging the process using light microscopy (fig. S2). Upon the initiation of assembly (time 0), the opaque solution primarily contained spheres of various sizes, reaching up to several micrometers in diameter. Over time, the capillary-enclosed solution became clearer as optical characteristics of a gel were observed concurrently with the appearance of elongated assemblies and the disappearance of the spheres. Finally, crystals were observed in the capillary.

TEM was used to provide more detailed information about the structural features of the assemblies at time 0 and after the formation of the gel. Examination of the structures at these time points confirmed the previous observations, revealing the dominant presence of spheres with diameters ranging from tens of nanometers to micrometers at the initial stage of assembly and the existence of a tangled network of fine fibrils in the semitransparent gel-like state (Fig. 1C). Together, the macroscopic and light and electron microscopy observations are consistent with a previously reported sphere-to-fiber transition of another LMW Fmoc-containing hydrogelator (*38*).

To assess the dynamics and stability of the formed structures throughout the assembly process in solution, with minimum preparation-related artifacts, we used cryogenic TEM (cryo-TEM). Samples for cryo-TEM were taken at different time points after the initiation of assembly (Fig. 2 and fig. S3). Micrographs of time 0 samples, taken when the solution was opaque, revealed a heterogeneous population of spheres of various sizes. These spheres appeared to be soft and were capable of adhering to the carbon-coated grid, forming menisci at the point of adhesion. Moreover, the spheres seemed to be hollow, occasionally encapsulating additional spheres inside them. Micrographs of samples that were taken during the first hour after the initiation of assembly, when the solution was still turbid, showed a mixed population of spheres, single- and multistrand fibers, and twisted ribbons. A similar mixture of assemblies appeared in samples taken 2 and 4 hours following the initiation of assembly, after the preparation had transformed into a weak semitransparent gel; however, at these time points, the diameter of the spheres was smaller, and the fibers formed a tangled network, as expected for the gel state. The observation of the dynamic spherical material is unique as compared to a previously reported study of Fmoc-DOPA assemblies (*32*). We assume that the metastability of the spherical material plays a major role in the distinctive structural transition observed in this system, as is further supported by the solution and ssNMR analyses described below. Additional major microscopic transition in the samples occurred over the following days, when tubes and helical ribbons appeared in addition to the fibrillar and spherical assemblies detected previously; notably, the spheres seemed to have further decreased in size, with a typical diameter smaller than 20 nm. Finally, micrographs of samples taken 1.5 months after the initiation of assembly, when crystals were macroscopically observable, again revealed the existence of helical ribbons and tubes. Because particular morphologies in the Fmoc-DOPA system emerge at the expense of others over time, the morphological transition exhibited by this system can therefore be considered hierarchical. Hierarchical, time-dependent formation of nanostructures was previously reported, mainly in the context of chiral amphiphilic peptide systems (*19*, *20*, *39*, *40*). Pertinent to this is the morphological transition from twisted to helical ribbons that generally occurs as part of a path to the formation of tubes (*20*, *39*, *41*); as described, such a transition was observed in the Fmoc-DOPA system as well. The current report of the Fmoc-DOPA system is exclusive

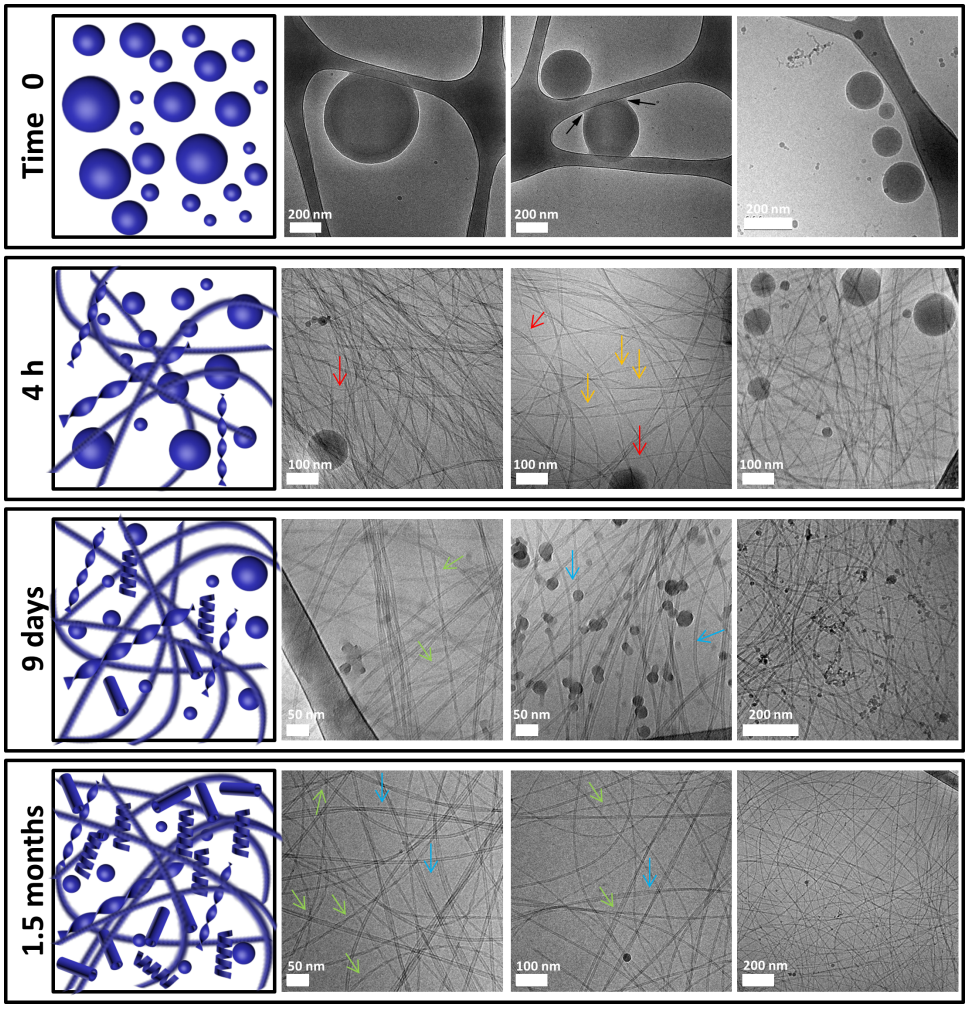

Fig. 2. Cryo-TEM analysis of Fmoc-DOPA assembly. Samples of Fmoc-DOPA (1 mg/ml) were imaged using cryo-TEM at different time points after the initiation of assembly. Micrographs of time 0 are from samples of a turbid solution. Micrographs of 4 hours and 9 days are from semitransparent gel-like samples. Micrographs of 1.5 months are from a gel containing macroscopically observable crystals. Black arrows point to spheres that adhere to the carbon-coated grid, forming menisci at the point of adhesion. Red arrows point to fibers. Orange arrows point to twisted ribbons. Green arrows point to helical ribbons. Blue arrows point to tubes.

because all stages, including the occurrence of metastable spheres and single crystals in addition to various fibrillar and tubular morphologies, are present and thoroughly investigated.

Spectroscopic studies of a phase transition process

To gain insight into the molecular events underlying the observed macroscopic and morphological transitions, vibrational and electronic spectroscopic assays were used. As described, an important early stage in the Fmoc-DOPA system is the sphere-to-fiber morphological transition that is accompanied by a sol-gel phase transition. Because the formation of a fibrillar network is the main driving force for gelation and considering the chiral nature of supramolecular fibrillar assemblies, we used near-UV time-dependent circular dichroism (CD) spectroscopy to monitor the gelation process; this was done in conjunction with a qualitative vial inversion assay (Fig. 3A). Because of the high turbidity of the Fmoc-DOPA solution, we could not collect CD spectra during the first hour of assembly. Approximately 70 min after the initiation of assembly, weak negative ellipticity was observed near 305 nm. As indicated by the vial inversion assay, the onset of gelation was shortly thereafter, approximately 90 min after the initiation of assembly. At later time points, the CD spectra maintained their features, yet the intensity of the 305-nm band increased; specifically, the intensity remained similar between 2 and 6 hours after the initiation of assembly, and a substantial increase was measured only after extended periods of time (9 days and 1.5 months). The 305-nm CD band is characteristic of parallel-displaced π-stacking of Fmoc moieties that occurs in the fibrillar assemblies (*36*, *42*, *43*). The high intensity of this band at the later time points may be attributed to an increased population of helical ribbons and tubes, as was made evident by cryo-TEM. Temperature-dependent CD analysis (Fig. 3B) confirmed that the 305-nm band could be ascribed to such intermolecular interactions because the band diminished at elevated temperatures, indicating that a molecularly dissolved state had been reached. This observation is in line with a previous report regarding the Fmoc-DOPA system (*32*).

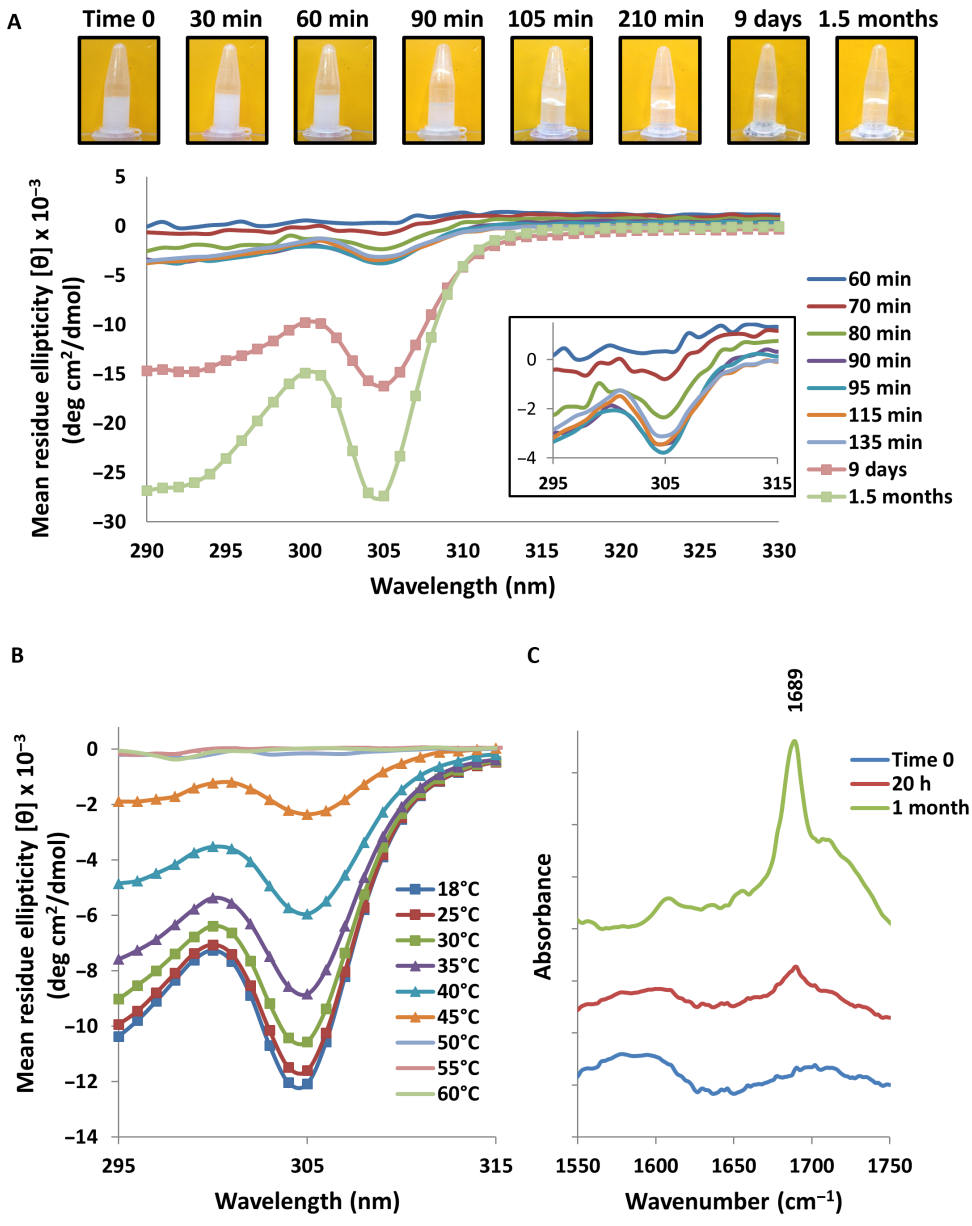

Fig. 3. Spectroscopic investigation of Fmoc-DOPA assembly. (**A**) Near-UV time-dependent CD spectra of Fmoc-DOPA (1 mg/ml) and a corresponding macroscopic vial inversion assay. The inset shows a magnification of the CD spectra collected between 295 and 315 nm during the first hours of assembly. (**B**) Temperature-dependent CD spectra of Fmoc-DOPA (1 mg/ml). (**C**) Fourier transform infrared (FTIR) spectra of the amide I′ region for Fmoc-DOPA samples (1 mg/ml) taken at different time points. FTIR spectra were normalized and vertically offset for clarity.

To further investigate the changes in the molecular packing of Fmoc-DOPA throughout the phase transition process, FTIR spectroscopy was used. Spectra were collected upon the initiation of assembly, at 20 hours when the preparation was gel-like and after 1 month when crystals were observable. The amide I′ region of the FTIR spectra contained a pronounced band at 1689 cm^{-1} for the samples taken at 20 hours and at 1 month, with significant sharpening and higher relative intensity in the case of the 1-month sample (Fig. 3C). A band near 1680 to 1695 cm^{-1} was recently attributed to stacked carbamate groups in supramolecular assemblies of Fmoc peptides (*44*–*46*). Therefore, the observed 1689 cm^{-1} band indicates that in the gel phase of the Fmoc-DOPA system, regardless of the existence of crystals, the Fmoc group drives the packing of Fmoc-DOPA into fibrillar assemblies in a process mediated by hydrophobic and aromatic interactions; this is in line with the findings of Mezzenga and co-workers (*32*). Moreover, the sharpening and increased intensity of the 1689 cm^{-1} band suggest that a larger portion of Fmoc-DOPA molecules are arranged in well-organized assemblies at later time points, well after the initial gelation. These assemblies are most probably of fibrillar nature, as shown by cryo-TEM.

Mechanism of Fmoc-DOPA assembly based on NMR and x-ray crystallography

The molecular packing of Fmoc-DOPA that underlies the sol-gel-crystal phase transition process was further probed by ^{1}H solution and

ssNMR. Upon the initiation of assembly, hydrophobic interactions most likely drive the assembly process into spherical structures without a high inner-order organization as observed in other amphiphiles (*22*). As described above, we assume that the formed spheres are metastable. The spheres most likely undergo disassembly into monomeric Fmoc-DOPA building blocks, which are presumably engaged in solvent interactions that result in a high degree of disorder and dynamic fluctuation. To discern the nature of the local molecular environment of Fmoc-DOPA molecules over time, we first monitored the assembly process with ^{1}H solution NMR. Figure 4A shows the one-dimensional (1D) ^{1}H solution spectra taken at different time points where, for clarity, we expanded the spectra to display the aromatic region; it should be noted though that this behavior is relatively uniform across all resonances (fig. S4A). The initial time 0 spectrum, corresponding to the time point dominated by the spherical structures, exhibits broad spectral features throughout the entire spectrum. This implies that each resonance is experiencing a distribution of local chemical shift environments facilitated by dynamic exchange. On the time scales where the dominant morphologies observed by cryo-TEM are fibrillar, the local structures become more homogeneous, as evidenced by the emergence of the sharp spectral features in the 5-hour spectrum and their increased prominence at the later times. However, even at 20 hours, when the dominant morphologies are fibrillar, the broad base still persists, indicating that dynamic processes are still occurring and that a diverse population of assemblies still exists. The latter point is further supported by the slight chemical shift differences observed in the narrow spectral features at each resonance. This evidence supports the notion of a dynamic molecular environment, facilitated by solvent interactions.

To assess the importance of solvent in the structure, we turned to ssNMR characterization. For this, we lyophilized the assemblies at different time points and recorded 1D solid-state ^{1}H spectra at 60-kHz magic angle spinning (MAS) on the resulting powder (fig. S4B). The spectra observed at the early stage, during the first hours of assembly, remain largely unresolved even under 60-kHz MAS, which is typical of highly amorphous rigid solid systems, implying that after solvent removal, the molecules collapse into largely unspecific amorphous morphologies. This is supported by high-resolution scanning electron microscopy (HR-SEM) and powder x-ray diffraction (XRD), which show the structural collapse after lyophilization at the early stage (fig. S5). These results confirm the significant role of solvent in facilitating dynamics and the structural shifts even for the fibrillar assemblies. For the much

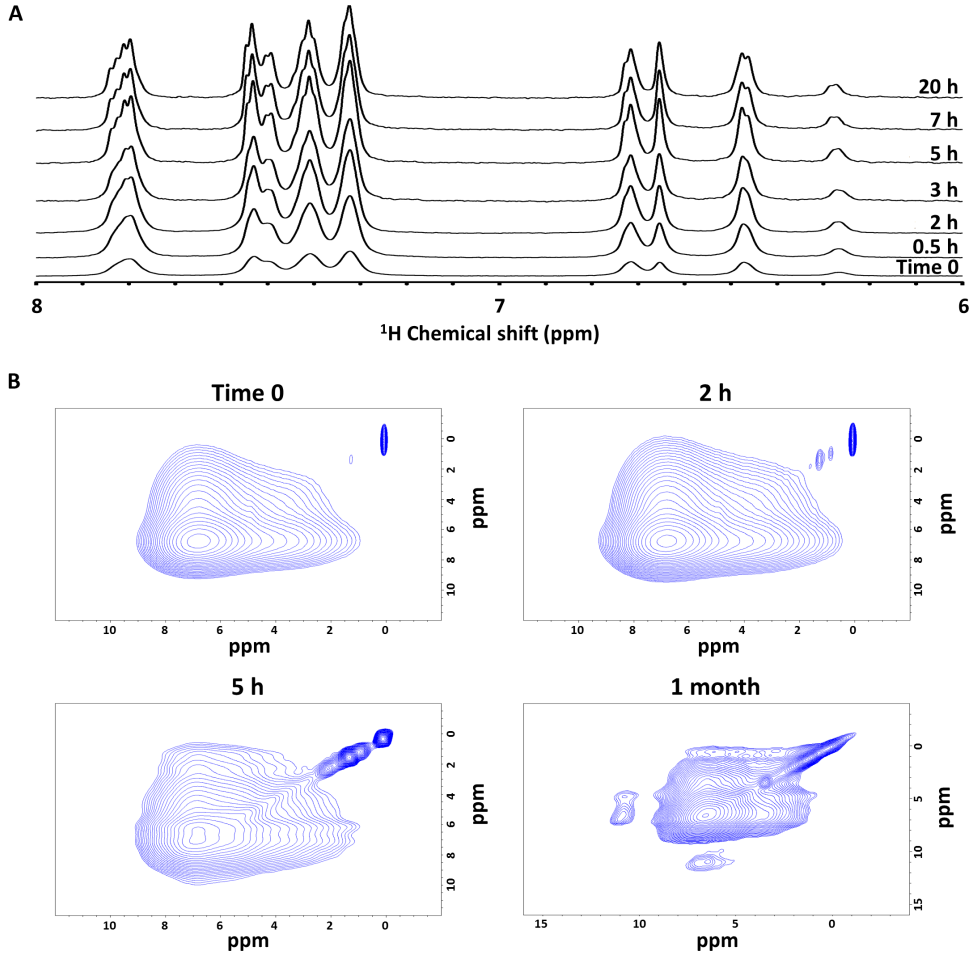

Fig. 4. NMR structural analysis of Fmoc-DOPA assemblies. (**A**) 1D ^{1}H NMR spectra of Fmoc-DOPA assembly by solution NMR at different time points. (**B**) 2D ^{1}H radio frequency–driven recoupling (RFDR) data of lyophilized Fmoc-DOPA samples prepared immediately (time 0), 2 hours, 5 hours, and 1 month after the assembly was initiated.

later time point of 1 month, which is on the time scale of crystal formation, significant changes were observed in the 1D spectrum. Although the dominant phenyl peak of the Fmoc moiety remains broad, small singularities are observed in the aliphatic region along with the emergence of a new peak at 11 parts per million (ppm). The new peak is an overlap of the OH protons originating from the DOPA portion of the molecule. All new features, as well as the HR-SEM and powder XRD results of a corresponding lyophilized preparation (fig. S5), point to a more homogeneous structure, as expected from the crystal. The fact that the 11-ppm peak is unobservable at the earlier time points affirms again that these early structures are amorphous. Furthermore, this suggests that this peak is more significant for the DOPA portion of the molecule, which is the likely molecular moiety to be involved in solvent interactions and the last to be involved in the final thermodynamically stable crystal. We then turned to RFDR, a powerful 2D correlation experiment, which allows spins to communicate via a spin flip-flop mechanism facilitated by the through-space dipolar couplings. Figure 4B shows the 2D $^{1}H/^{1}H$ RFDR spectra for early and 1-month assembly time points. As expected, the early time points are dominated by a large featureless correlation centered about the aromatic peak. The nonselectivity of the cross peaks here again confirms the amorphous structure of the early assemblies. For the 1-month spectrum, however, one can observe an additional cross peak between the OH (10 ppm) and aromatic (5 to 6 ppm) resonances. The appearance of this peak shows that the DOPA is stabilized and oriented, a stage which is driven by hydrogen bonds, as revealed in the crystal structure.

As mentioned above, the phase transition process in the Fmoc-DOPA system culminates in the formation of crystals. Spontaneous crystallization of Fmoc-DOPA occurred at a range of concentrations and varying ratios of water and ethanol (fig. S6). The crystal structure of Fmoc-DOPA was determined by XRD at 0.80 Å resolution. The determined structure belongs to a monoclinic crystal system, space group $P2_1$, with one molecule per asymmetric unit. In contrast to the predominant π-stacking interactions of the Fmoc groups, which mediate the packing of Fmoc-DOPA into fibrillar assemblies at the gel phase, the crystal structure of Fmoc-DOPA is mainly stabilized by a network of hydrogen bonds and herringbone face/edge aromatic interactions (Fig. 5 and table S1). The stabilization of the DOPA moiety by hydrogen bonds is in line with the ssNMR analysis for the 1-month sample, and the resulting "locking" effect is crucial for the conclusion of the transition process exhibited by the Fmoc-DOPA system. The crystal structure of other Fmoc-protected amino acids was previously reported (*47*–*51*). A spontaneous gel-crystal transition of another LMW hydrogelator was reported as well (*52*) and so has the spontaneous gel-crystal transition of naphthalene (Nap)–modified LMW hydrogelator (*53*). Similar to our observation, the molecular packing of the Nap-modified building blocks in the gel phase differs from the one observed in the crystal phase. Parallel work by Adams and co-workers (*54*) also demonstrated this by investigating the gel-crystal transition of the related

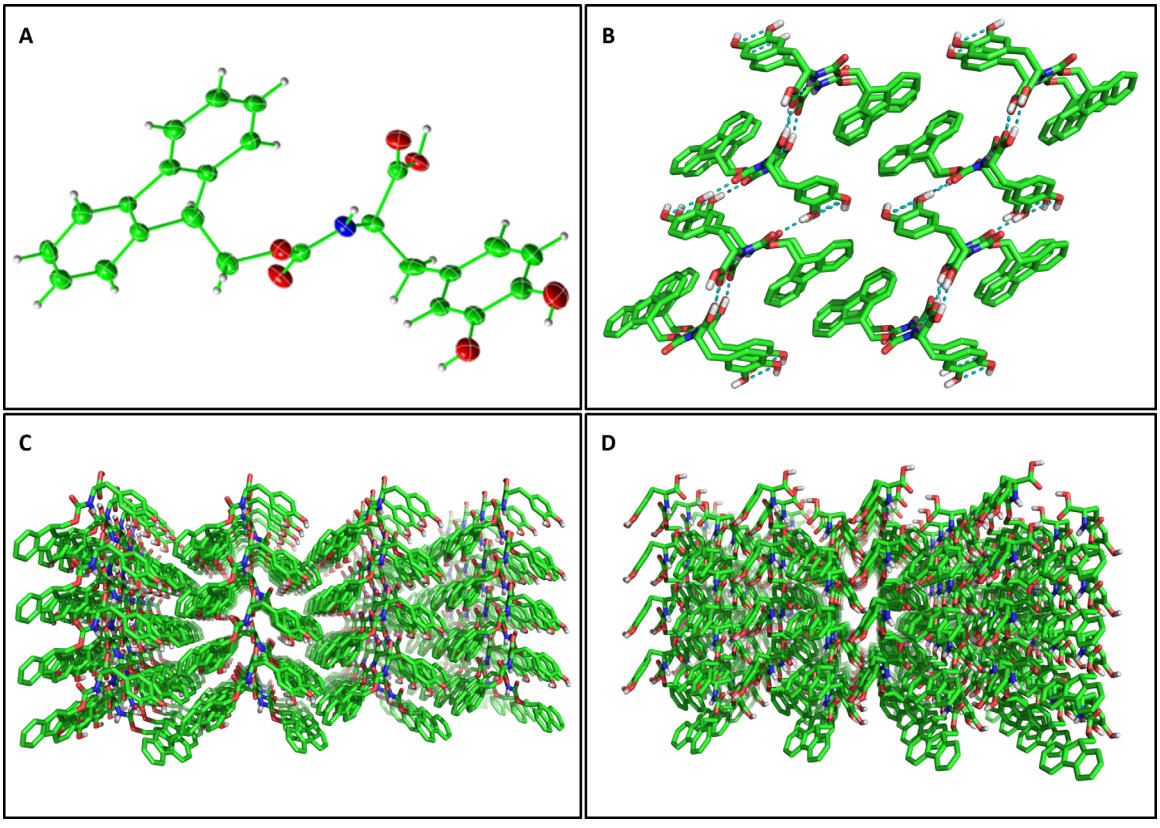

Fig. 5. X-ray structure of Fmoc-DOPA single crystals. (**A**) View of the asymmetric unit, showing a single Fmoc-DOPA molecule with thermal ellipsoids at 50% probability level. (**B**) Crystal packing of 16 molecules along the crystallographic *b* axis. The interlocking hydrogen bonding network is shown in teal. (**C**) Extended crystal packing along the crystallographic *a* axis. (**D**) Extended crystal packing along the crystallographic *c* axis.

Fmoc-Tyr hydrogelator, which exhibited a marked difference between the two phases in the packing of the building blocks. In contrast, the Fmoc-Phe gel and crystal phases, which were also investigated in the work mentioned above, were deemed similar in their molecular packing. Together, this suggests that in such systems, a comprehensive structural rearrangement often leads to the formation of the ultimate ultrastructures (*55*) and that this rearrangement underlies the final stage in the phase transition process. It is worth mentioning that Adams and co-workers (*56*) recently reported a gel-crystal transition of the Fmoc-Phe-Phe hydrogelator. It was argued that the interpretation of the single-crystal structure of Fmoc-Phe-Phe is not informative for determining the packing of the fibrous structures in the gel, as was also claimed in their previous report (*53*). These observations are in line with the current findings regarding the Fmoc-DOPA system.

CONCLUSIONS

We have observed and dissected the Fmoc-DOPA system and consider it to be a minimal multiphase model for supramolecular polymers in which diverse molecular forces participate at the different stages of structural transitions. On the basis of our multiscale analysis, we propose a model for the Fmoc-DOPA assembly process (Fig. 6). This process is characterized by three distinct and important stages: (i) hydrophobic association in solution as in classical amphiphiles; (ii) organization into ordered fibrillar assemblies at the nanoscale, mediated by the arrangement of the aromatic Fmoc and DOPA moieties; and (iii) crystallization that mainly results from spatial locking and stabilization by hydrogen bonds. These stages reflect general properties of supramolecular polymer systems, yet are manifested here by a simple, minimalistic building block.

Specifically, upon the initiation of assembly, molecularly dissolved Fmoc-DOPA building blocks rearrange into metastable spheres, similarly to the general organization of amphiphilic molecules in solution. These spheres continuously maintain equilibrium with their monomeric building blocks that serve as a reservoir from which supramolecular assemblies in the gel phase are formed. At this very early stage, the assembly is mainly mediated by hydrophobic interactions, the molecular arrangement of the Fmoc moieties is nonspecific, and the molecules remain dynamic. The sol-gel transition involves the aromatic packing of free monomers into well-defined fibrillar assemblies of different morphologies. Because of the geometrically restricted interactions between aromatic moieties, the assemblies become more homogeneous and exhibit more persistent long-range order, yet solvent and dynamics still play a major role. The disordered aspects of the spheres and the fibrillar assemblies are a kinetically driven product that arises from dynamic competition and interaction with solvent molecules. Finally, in the solid crystals that emerge at later time points, a network of hydrogen bonds between DOPA moieties leads to the locking of Fmoc-DOPA molecules in a thermodynamically favorable ultrastructure.

To conclude, we have thoroughly investigated the Fmoc-DOPA, a simple building block that can serve as a minimal model for the experimental study of supramolecular polymers. Because supramolecular polymers are of growing interest for various applications, this is the simplest representation of such an important class of noncovalent biomolecular assemblies. The unique structure of the systems facilitated the deconvolution of the various aspects of assembly and allowed the high-resolution monitoring of common phenomena that were not fully understood, such as the opacity to transparent transition of such nanosystems. Moreover, our establishment of the multiphase and diverse interactions that facilitate the assembly process, together with the remarkably small size of this building block, makes it very attractive for further exploration of this specific system by experimental studies as well as by molecular dynamics and quantum chemistry computational analysis, including density function theory. Thus, the identification and validation of this minimalistic model could pave the way for better comprehension of molecular self-assembly into functional supramolecular polymers also at the subatomic quantum level.

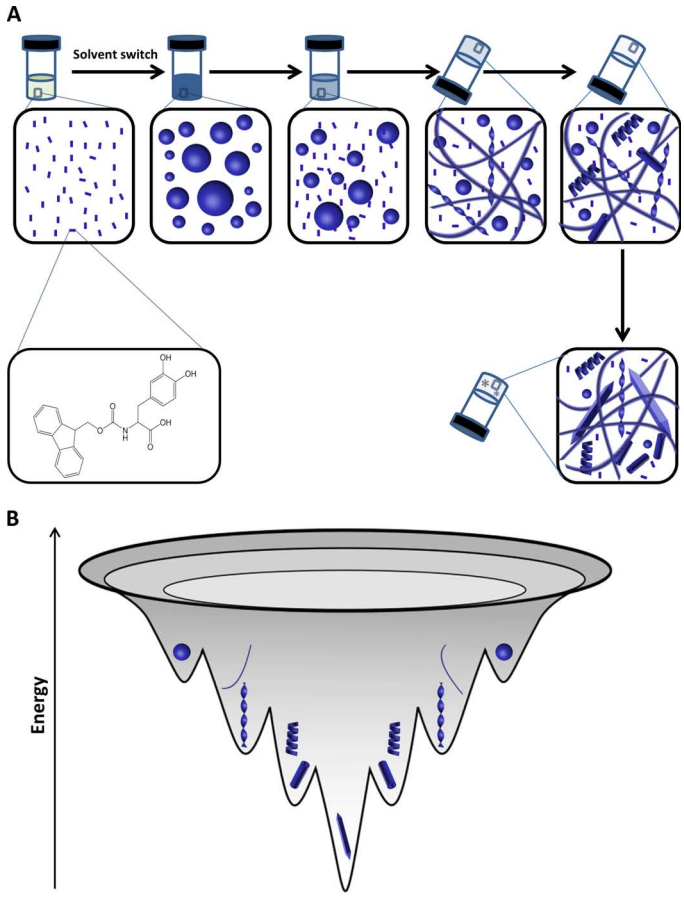

Fig. 6. Suggested model for the Fmoc-DOPA structural transition process. (**A**) Schematic diagram showing a sol-gel-crystal transition that occurs at the macroscopic level, with an underlying morphological transition at the microscopic level. This process includes a morphological transition from spheres into fibers and twisted ribbons, and finally into helical ribbons and tubes. (**B**) Energy landscape of the Fmoc-DOPA transition process. This process involves the transition of metastable spheres into thermodynamically favorable crystalline ultrastructure.

MATERIALS AND METHODS

Preparation of Fmoc-DOPA assemblies

Fmoc-DOPA (>95% purity) was purchased from AnaSpec Inc. The material identity was confirmed by mass spectrometry. For the formation of Fmoc-DOPA assemblies, lyophilized Fmoc-DOPA was dissolved in

ethanol to a concentration of 100 mg/ml, then diluted with double-distilled water to a final concentration of 1 mg/ml and incubated at 18°C.

Turbidity assay

Samples of Fmoc-DOPA were prepared as described above and then immediately transferred to a capped rectangular quartz cuvette with an optical path length of 0.1 cm. The short path length enabled the monitoring of solution turbidity from time 0. Optical density at 350 nm was measured at 5-min intervals over a time period of 7 hours using a Chirascan spectrometer (Applied Photophysics) fitted with a Peltier temperature controller set to 18°C. The experiment was repeated three times and the results were averaged.

Capillary assay

A sample of Fmoc-DOPA was prepared as described above, immediately inserted into a rectangular glass capillary (CM Scientific), sealed, and then observed using an ML8100 light microscope (Meiji Techno) over time.

Transmission electron microscopy

TEM analysis was performed by applying 10-μl samples to 400-mesh copper grids covered by carbon-stabilized formvar film (Electron Microscopy Science). The samples were allowed to adsorb for 2 min before excess fluid was blotted. To negatively stain the samples, 10 μl of 2% uranyl acetate was then deposited on the grid and allowed to adsorb for 2 min before excess fluid was blotted. TEM micrographs were recorded using JEOL 1200EX electron microscope operating at 80 kV.

Cryo-TEM analysis

Specimens of Fmoc-DOPA assemblies were prepared in a controlled environment vitrification system at 18°C and 100% relative humidity (*57*). Vitrified specimens were examined by a Philips CM120 or a FEI T12 G2 transmission electron microscopes operated at 120 kV, with Oxford CT-3500 or Gatan 626 cooling holders and transfer stations. Specimens were equilibrated in the microscope below −178°C and then examined in the low-dose imaging mode to minimize electron-beam radiation damage. Images were recorded at a nominal underfocus of 1 to 2 μm to enhance phase contrast. Images were acquired digitally by a Gatan MultiScan 791 (CM120) or Gatan US1000 high-resolution (T12) cooled-CCD camera using the Digital Micrograph software package.

Circular dichroism spectroscopy

CD spectra were collected with a Chirascan spectrometer (Applied Photophysics) fitted with a Peltier temperature controller, using a capped rectangular quartz cuvette with an optical path length of 1 mm. Data acquisition was performed in steps of 1 nm at the range of 290 to 375 nm, with a spectral bandwidth of 1 nm and an averaging time of 1 s. Absorbance was monitored and kept under 2 u for all measurements. To monitor the assembly kinetics, fresh Fmoc-DOPA solution (1 mg/ml) was prepared as described above and the CD spectrum was collected at 18°C at 5-min intervals for a duration of 6 hours and at later points as required. To assess the thermal stability of the assemblies, Fmoc-DOPA solution (1 mg/ml) in water was prepared and stored at 18°C for approximately 48 hours. CD spectra were then collected at 18°C and at 25° to 60°C in an ascending 5°C stepped ramp. The solution was allowed to equilibrate for 15 min at every temperature point before measurement. The signals were normalized to mean residue ellipticity (*58*). To verify whether the assayed solution contained characteristic assemblies, a 10-μl sample of the cuvette content was examined by TEM as described above.

Fourier transform infrared spectroscopy

FTIR spectroscopy was performed with 30-μl samples of Fmoc-DOPA solutions (1 mg/ml) prepared as described above, but the concentrated stock solution was diluted into D_2O (99.8%; Sigma-Aldrich). The samples were deposited onto disposable KBr IR sample cards (Sigma-Aldrich), which were then allowed to dry under vacuum. Transmission infrared spectra were collected using Nexus 470 FTIR spectrometer (Nicolet) with a deuterated triglycine sulfate detector. Measurements were performed using the atmospheric suppression mode by averaging 64 scans in 2 cm^{-1} resolution.

Nuclear magnetic resonance

1D ^1H solution spectra were obtained on a 600-MHz Bruker Avance spectrometer equipped with a triple resonance cryogenic probe using a simple 1D pulse sequence with Watergate suppression. All solid-state experiments were done on a Varian 600-MHz spectrometer using a 1.2-mm 60-kHz MAS probe. The 1D ^1H and 2D $^1H/^1H$ RFDR (*59*, *60*) experiments were obtained under 60-kHz MAS. The RFDR data reported were all obtained with a 6.6-ms mixing time. The samples for solid-state experiments were prepared by initiating assembly via the standard procedure before freezing the solution with liquid nitrogen at the time points of interest followed by lyophilization for at least 24 hours. Once all the solvent was extracted, the lyophilized powder was packed immediately into a 1.2-mm rotor. Between experiments, the rotor was stored at −20°C.

High-resolution scanning electron microscopy

To image solution samples, 5-μl samples of Fmoc-DOPA (1 mg/ml), taken at different time points, were dried at room temperature on microscope glass coverslips. To image the powder of lyophilized Fmoc-DOPA assemblies, samples of Fmoc-DOPA (1 mg/ml), taken at different time points, were flash-frozen in liquid nitrogen and lyophilized for at least 20 hours. All samples were coated with approximately 30 nm of Cr. Images were taken using a JEOL JSM-6700F FE-SEM operating at 10 kV.

Powder x-ray diffraction

Samples were prepared as described above and at specific time points, flash-frozen with liquid nitrogen, and lyophilized for at least 24 hours. XRD data were collected in symmetric Bragg-Brentano geometry with CuKα radiation on a Bruker D8 Discover X-ray diffractometer equipped with a 1D LynxEye detector based on compound silicon strip technology. Quantitative processing was performed with JADE 9.6 (MDI) software.

Single-crystal x-ray structure determination

A colorless needle of dimensions 0.3 × 0.05 × 0.02 mm was transferred to Hampton Paratone oil, mounted on a MiTeGen loop, and flash-frozen in liquid nitrogen stream. X-ray data were collected at 100 K on a Bruker Kappa Apex II diffractometer with MoKα (λ = 0.71703 Å) equipped with a graphite monochromator and MiraCol Optics. Data were collected at 0.5° frames, 240 s/deg. A total of 744 frames were collected. Frames were integrated with the Bruker SAINT software package. Data were collected to a $2\theta_{max}$ = 52.74° with limiting indices $-15 \le h \le 15$, $-7 \le k \le 5$, $-18 \le l \le 16$, yielding a total of 8594

reflections, of which 3220 were independent (average redundancy, 2.7; completeness, 98.3%; R_{int} = 7.24%).

The structure was solved and refined using SHELXTL software in Monoclinic space group $P2_1$, with Z = 2. Atoms were refined anisotropically with the exception of hydrogen atoms that were placed in calculated positions and refined in riding mode.

Full-matrix least-squares refinement based on F^2 with SHELXL-97 on 290 parameters with one restraint gave final R_1 = 0.0535 (based on F^2) for data with $I > 2\sigma(I)$, and R_1 = 0.1134 on 3220 reflections, goodness-of-fit on F^2 = 0.974, largest electron density peak 0.45 e Å^{-3}, and the largest hole –0.270 e Å^{-3}. Crystal data collection and refinement parameters are given in table S2. Coordinates for the structure can be found in the supplemental crystallographic information file.

SUPPLEMENTARY MATERIALS

Supplementary material for this article is available at http://advances.sciencemag.org/cgi/content/full/2/2/e1500827/DC1

Fig. S1. Turbidity assay to monitor Fmoc-DOPA optical transition over time.
Fig. S2. Sealed capillary assay to monitor Fmoc-DOPA assembly.
Fig. S3. Cryo-TEM of Fmoc-DOPA assemblies at additional time points.
Fig. S4. Additional NMR analysis of Fmoc-DOPA assembly.
Fig. S5. The influence of lyophilization on the assemblies.
Fig. S6. Exploring Fmoc-DOPA phase transition.
Table S1. Hydrogen bonding parameters from Fmoc-DOPA crystal structure.
Table S2. Crystal data and structure refinement for the Fmoc-DOPA crystal.

REFERENCES AND NOTES

1. S. I. Stupp, V. LeBonheur, K. Walker, L. S. Li, K. E. Huggins, M. Keser, A. Amstutz, Supramolecular materials: Self-organized nanostructures. *Science* **276**, 384–389 (1997).
2. L. Brunsveld, B. J. B. Folmer, E. W. Meijer, R. P. Sijbesma, Supramolecular polymers. *Chem. Rev.* **101**, 4071–4098 (2001).
3. J.-M. Lehn, Toward complex matter: Supramolecular chemistry and self-organization. *Proc. Natl. Acad. Sci. U.S.A.* **99**, 4763–4768 (2002).
4. S. Zhang, Fabrication of novel biomaterials through molecular self-assembly. *Nat. Biotechnol.* **21**, 1171–1178 (2003).
5. T. Aida, E. W. Meijer, S. I. Stupp, Functional supramolecular polymers. *Science* **335**, 813–817 (2012).
6. M. C. Branco, D. M. Sigano, J. P. Schneider, Materials from peptide assembly: Towards the treatment of cancer and transmittable disease. *Curr. Opin. Chem. Biol.* **15**, 427–434 (2011).
7. L. Adler-Abramovich, E. Gazit, The physical properties of supramolecular peptide assemblies: From building block association to technological applications. *Chem. Soc. Rev.* **43**, 6881–6893 (2014).
8. X. Du, J. Zhou, B. Xu, Supramolecular hydrogels made of basic biological building blocks. *Chem. Asian J.* **9**, 1446–1472 (2014).
9. S.-J. Rymer, S. J. B. Tendler, C. Bosquillon, C. Washington, C. J. Roberts, Self-assembling peptides and their potential applications in biomedicine. *Ther. Deliv.* **2**, 1043–1056 (2011).
10. Y. Ikezoe, G. Washino, T. Uemura, S. Kitagawa, H. Matsui, Autonomous motors of a metal–organic framework powered by reorganization of self-assembled peptides at interfaces. *Nat. Mater.* **11**, 1081–1085 (2012).
11. C. A. E. Hauser, S. Maurer-Stroh, I. C. Martins, Amyloid-based nanosensors and nanodevices. *Chem. Soc. Rev.* **43**, 5326–5345 (2014).
12. Y. Liu, Z. Wang, X. Zhang, Characterization of supramolecular polymers. *Chem. Soc. Rev.* **41**, 5922–5932 (2012).
13. A. Mitraki, Protein aggregation: From inclusion bodies to amyloid and biomaterials. *Adv. Protein Chem. Struct. Biol.* **79**, 89–125 (2010).
14. E. Gazit, The "correctly folded" state of proteins: Is it a metastable state? *Angew. Chem. Int. Ed. Engl.* **41**, 257–259 (2002).
15. S. Auer, M. A. Miller, S. V. Krivov, C. M. Dobson, M. Karplus, M. Vendruscolo, Importance of metastable states in the free energy landscapes of polypeptide chains. *Phys. Rev. Lett.* **99**, 178104 (2007).
16. A. J. Baldwin, T. P. J. Knowles, G. G. Tartaglia, A. W. Fitzpatrick, G. L. Devlin, S. L. Shammas, C. A. Waudby, M. F. Mossuto, S. Meehan, S. L. Gras, J. Christodoulou, S. J. Anthony-Cahill, P. D. Barker, M. Vendruscolo, C. M. Dobson, Metastability of native proteins and the phenomenon of amyloid formation. *J. Am. Chem. Soc.* **133**, 14160–14163 (2011).
17. S. Ogi, K. Sugiyasu, S. Manna, S. Samitsu, M. Takeuchi, Living supramolecular polymerization realized through a biomimetic approach. *Nat. Chem.* **6**, 188–195 (2014).
18. J. H. Ortony, C. J. Newcomb, J. B. Matson, L. C. Palmer, P. E. Doan, B. M. Hoffman, S. I. Stupp, Internal dynamics of a supramolecular nanofibre. *Nat. Mater.* **13**, 812–816 (2014).
19. E. T. Pashuck, S. I. Stupp, Direct observation of morphological tranformation from twisted ribbons into helical ribbons. *J. Am. Chem. Soc.* **132**, 8819–8821 (2010).
20. L. Ziserman, H.-Y. Lee, S. R. Raghavan, A. Mor, D. Danino, Unraveling the mechanism of nanotube formation by chiral self-assembly of amphiphiles. *J. Am. Chem. Soc.* **133**, 2511–2517 (2011).
21. A. Levin, T. O. Mason, L. Adler-Abramovich, A. K. Buell, G. Meisl, C. Galvagnion, Y. Bram, S. A. Stratford, C. M. Dobson, T. P. J. Knowles, E. Gazit, Ostwald's rule of stages governs structural transitions and morphology of dipeptide supramolecular polymers. *Nat. Commun.* **5**, 5219 (2014).
22. A. Sorrenti, O. Illa, R. M. Ortuño, Amphiphiles in aqueous solution: Well beyond a soap bubble. *Chem. Soc. Rev.* **42**, 8200–8219 (2013).
23. H. Matsui, B. Gologan, Crystalline glycylglycine bolaamphiphile tubules and their pH-sensitive structural transformation. *J. Phys. Chem. B* **104**, 3383–3386 (2000).
24. S. Fleming, R. V. Ulijn, Design of nanostructures based on aromatic peptide amphiphiles. *Chem. Soc. Rev.* **43**, 8150–8177 (2014).
25. G. Fichman, L. Adler-Abramovich, S. Manohar, I. Mironi-Harpaz, T. Guterman, D. Seliktar, P. B. Messersmith, E. Gazit, Seamless metallic coating and surface adhesion of self-assembled bioinspired nanostructures based on di-(3,4-dihydroxy-L-phenylalanine) peptide motif. *ACS Nano* **8**, 7220–7228 (2014).
26. D. J. Adams, Dipeptide and tripeptide conjugates as low-molecular-weight hydrogelators. *Macromol. Biosci.* **11**, 160–173 (2011).
27. X. Yan, P. Zhu, J. Li, Self-assembly and application of diphenylalanine-based nanostructures. *Chem. Soc. Rev.* **39**, 1877–1890 (2010).
28. P. W. J. M. Frederix, R. V. Ulijn, N. T. Hunt, T. Tuttle, Virtual screening for dipeptide aggregation: Toward predictive tools for peptide self-assembly. *J. Phys. Chem. Lett.* **2**, 2380–2384 (2011).
29. J. Shi, Y. Gao, Z. Yang, B. Xu, Exceptionally small supramolecular hydrogelators based on aromatic–aromatic interactions. *Beilstein J. Org. Chem.* **7**, 167–172 (2011).
30. P. W. J. M. Frederix, G. G. Scott, Y. M. Abul-Haija, D. Kalafatovic, C. G. Pappas, N. Javid, N. T. Hunt, R. V. Ulijn, T. Tuttle, Exploring the sequence space for (tri-)peptide self-assembly to design and discover new hydrogels. *Nat. Chem.* **7**, 30–37 (2015).
31. E. Gazit, Molecular self-assembly: Searching sequence space. *Nat. Chem.* **7**, 14–15 (2015).
32. A. Saha, S. Bolisetty, S. Handschin, R. Mezzenga, Self-assembly and fibrillization of a Fmoc-functionalized polyphenolic amino acid. *Soft Matter* **9**, 10239–10242 (2013).
33. Z. Yang, H. Gu, D. Fu, P. Gao, J. K. Lam, B. Xu, Enzymatic formation of supramolecular hydrogels. *Adv. Mater.* **16**, 1440–1444 (2004).
34. S. Sutton, N. L. Campbell, A. I. Cooper, M. Kirkland, W. J. Frith, D. J. Adams, Controlled release from modified amino acid hydrogels governed by molecular size or network dynamics. *Langmuir* **25**, 10285–10291 (2009).
35. S. Roy, A. Banerjee, Amino acid based smart hydrogel: Formation, characterization and fluorescence properties of silver nanoclusters within the hydrogel matrix. *Soft Matter* **7**, 5300–5308 (2011).
36. D. M. Ryan, S. B. Anderson, F. T. Senguen, R. E. Youngman, B. L. Nilsson, Self-assembly and hydrogelation promoted by F_5-phenylalanine. *Soft Matter* **6**, 475–479 (2010).
37. G. Fichman, E. Gazit, Self-assembly of short peptides to form hydrogels: Design of building blocks, physical properties and technological applications. *Acta Biomater.* **10**, 1671–1682 (2014).
38. L. Chen, J. Raeburn, S. Sutton, D. G. Spiller, J. Williams, J. S. Sharp, P. C. Griffiths, R. K. Heenan, S. M. King, A. Paul, S. Furzeland, D. Atkins, D. J. Adams, Tuneable mechanical properties in low molecular weight gels. *Soft Matter* **7**, 9721–9727 (2011).
39. J. Adamcik, V. Castelletto, S. Bolisetty, I. W. Hamley, R. Mezzenga, Direct observation of time-resolved polymorphic states in the self-assembly of end-capped heptapeptides. *Angew. Chem. Int. Ed. Engl.* **50**, 5495–5498 (2011).
40. T. Shimizu, M. Masuda, H. Minamikawa, Supramolecular nanotube architectures based on amphiphilic molecules. *Chem. Rev.* **105**, 1401–1443 (2005).
41. T. G. Barclay, K. Constantopoulos, J. Matisons, Nanotubes self-assembled from amphiphilic molecules via helical intermediates. *Chem. Rev.* **114**, 10217–10291 (2014).
42. B. Adhikari, J. Nanda, A. Banerjee, Multicomponent hydrogels from enantiomeric amino acid derivatives: Helical nanofibers, handedness and self-sorting. *Soft Matter* **7**, 8913–8922 (2011).
43. Z. Yang, H. Gu, Y. Zhang, L. Wang, B. Xu, Small molecule hydrogels based on a class of antiinflammatory agents. *Chem. Commun.* 208–209 (2004).
44. S. Fleming, P. W. J. M. Frederix, I. Ramos Sasselli, N. T. Hunt, R. V. Ulijn, T. Tuttle, Assessing the utility of infrared spectroscopy as a structural diagnostic tool for β-sheets in self-assembling aromatic peptide amphiphiles. *Langmuir* **29**, 9510–9515 (2013).
45. S. Fleming, S. Debnath, P. W. J. M. Frederix, T. Tuttle, R. V. Ulijn, Aromatic peptide amphiphiles: Significance of the Fmoc moiety. *Chem. Commun.* **49**, 10587–10589 (2013).
46. K. M. Eckes, X. Mu, M. A. Ruehle, P. Ren, L. J. Suggs, β Sheets not required: Combined experimental and computational studies of self-assembly and gelation of the ester-containing analogue of an Fmoc-dipeptide hydrogelator. *Langmuir* **30**, 5287–5296 (2014).

47. G. Valle, G. M. Bonora, C. Toniolo, Linear oligopeptides. 118. preferred conformations and modes of self-association of the fluoren-9-ylmethoxycarbonyl amino acid derivatives. *Can. J. Chem.* **62**, 2661–2666 (1984).
48. K. Yamada, D. Hashizume, T. Shimizu, *N*-(Fluoren-9-ylmethoxycarbonyl)-L-leucine. *Acta Crystallogr. Sect. E Struct. Rep. Online* **E64**, o1112 (2008).
49. K. Yamada, D. Hashizume, T. Shimizu, K. Deguchi, *N*-(Fluoren-9-ylmethoxycarbonyl)-L-isoleucine. *Acta Crystallogr. Sect. E Struct. Rep. Online* **E64**, o1533 (2008).
50. K. Yamada, D. Hashizume, T. Shimizu, *N*-(Fluoren-9-ylmethoxycarbonyl)-L-aspartic acid 4-*tert*-butyl ester. *Acta Crystallogr. Sect. E Struct. Rep. Online* **E65**, o2606–o2607 (2009).
51. K. Yamada, D. Hashizume, T. Shimizu, S. Ohki, S. Yokoyama, A solid-state ^{17}O NMR, X-ray, and quantum chemical study of *N*-α-Fmoc-protected amino acids. *J. Mol. Struct.* **888**, 187–196 (2008).
52. Y. Wang, L. Tang, J. Yu, Investigation of spontaneous transition from low-molecular-weight hydrogel into macroscopic crystals. *Cryst. Growth Des.* **8**, 884–889 (2008).
53. K. A. Houton, K. L. Morris, L. Chen, M. Schmidtmann, J. T. A. Jones, L. C. Serpell, G. O. Lloyd, D. J. Adams, On crystal versus fiber formation in dipeptide hydrogelator systems. *Langmuir* **28**, 9797–9806 (2012).
54. E. R. Draper, K. L. Morris, M. A. Little, J. Raeburn, C. Colquhoun, E. R. Cross, T. O. McDonald, L. C. Serpell, D. J. Adams, Hydrogels formed from Fmoc amino acids. *CrystEngComm* **17**, 8047–8057 (2015).
55. D. J. Adams, K. Morris, L. Chen, L. C. Serpell, J. Bacsa, G. M. Day, The delicate balance between gelation and crystallisation: Structural and computational investigations. *Soft Matter* **6**, 4144–4156 (2010).
56. J. Raeburn, C. Mendoza-Cuenca, B. N. Cattoz, M. A. Little, A. E. Terry, A. Z. Cardoso, P. C. Griffiths, D. J. Adams, The effect of solvent choice on the gelation and final hydrogel properties of Fmoc–diphenylalanine. *Soft Matter* **11**, 927–935 (2015).
57. Y. Talmon, Transmission electron microscopy of complex fluids: The state of the art. *Ber. Bunsenges. Phys. Chem.* **100**, 364–372 (1996).
58. N. J. Greenfield, Using circular dichroism spectra to estimate protein secondary structure. *Nat. Protoc.* **1**, 2876–2890 (2006).
59. Y. Nishiyama, R. Zhang, A. Ramamoorthy, Finite-pulse radio frequency driven recoupling with phase cycling for 2D ^{1}H/^{1}H correlation at ultrafast MAS frequencies. *J. Magn. Reson.* **243**, 25–32 (2014).
60. A. E. Bennett, C. M. Rienstra, J. M. Griffiths, W. Zhen, P. T. Lansbury Jr., R. G. Griffin, Homonuclear radio frequency-driven recoupling in rotating solids. *J. Chem. Phys.* **108**, 9463–9479 (1998).

Acknowledgments: We thank Y. Rosenberg for powder XRD analysis, M. Alexandroni for photography, and members of the Gazit laboratory for helpful discussions. **Funding:** This work was supported in part by grants from the Israeli National Nanotechnology Initiative and the Helmsley Charitable Trust for a Focal Technology Area on Nanomedicines for Personalized Theranostics (to E.G.) and the Marian Gertner Fellowship of the Marian Gertner Institute for Medical Nanosystems (to G.F.). **Author contributions:** G.F., L.A.-A., and E.G. conceived and designed the experiments. G.F. and T.G. planned and performed the experiments. J.D. and A.R. designed and performed the NMR experiments. J.S., E.K., and Y.T. designed and performed the cryo-TEM experiments. L.J.W.S. performed and analyzed the x-ray diffraction experiments. G.F., T.G., L.A.-A., and E.G. prepared the manuscript. All authors discussed the results and commented on the manuscript. **Competing interests:** A patent application was submitted by G.F., L.A.-A., and E.G. on "Self-assembled micro- and nano-structures" that contained DOPA residues. All other authors declare no competing interests. **Data and materials availability:** All data described in the paper are presented in this report and in the Supplementary Materials.

Submitted 23 June 2015
Accepted 30 November 2015
Published 12 February 2016
10.1126/sciadv.1500827

Citation: G. Fichman, T. Guterman, J. Damron, L. Adler-Abramovich, J. Schmidt, E. Kesselman, L. J. W. Shimon, A. Ramamoorthy, Y. Talmon, E. Gazit, Spontaneous structural transition and crystal formation in minimal supramolecular polymer model. *Sci. Adv.* **2**, e1500827 (2016).